Journal of Materials Chemistry A

A 1.51 V pH Neutral Redox Flow Battery towards Scalable Energy Storage

Journal:	*Journal of Materials Chemistry A*
Manuscript ID	TA-ART-02-2019-001469.R1
Article Type:	Paper
Date Submitted by the Author:	27-Feb-2019
Complete List of Authors:	Luo, Jian; Utah State University, Chemistry and Biochemistry Wu, Wenda; Utah State University, Chemistry and Biochemistry DeBruler, Camden; Utah State University, Chemistry and Biochemistry Hu, Bo; Utah State University, Chemistry and biochemistry Hu, Maowei; Utah State University, Chemistry and Biochemistry Liu, Tianbiao; Utah State University, Department of Chemistry & Biochemistry

A 1.51 V pH Neutral Redox Flow Battery towards Scalable Energy Storage

Jian Luo, Wenda Wu, Camden Debruler, Bo Hu, Maowei Hu, T. Leo Liu*
The Department of Chemistry and Biochemistry, Utah State University, Logan, Utah 84322, USA
*Corresponding Author: Leo.Liu@usu.edu

Abstract: Aqueous redox flow batteries using low-cost organic and inorganic active materials have received growing interest for sustainable energy storage. In this study, low-cost, high redox potential (1.08 V vs NHE) and high capacity ammonium bromide (NH_4Br, 214.4 Ah/L) catholyte was coupled with the organic viologen anolyte to demonstrate 1.51 V high voltage $(SPr)_2V/Br^-$ aqueous redox flow batteries under pH neutral conditions for the first time. Benefitted from the high water solubility of both NH_4Br catholyte and $(SPr)_2V$ anolyte, the newly designed $(SPr)_2V/Br^-$ organic flow battery was operated at up to 1.5 M and an energy density of up to 30.4 Wh/L. Using multiwall carbon nanotubes as electrochemical additive for Br_3^-/Br^- redox couple, the highly energy dense $(SPr)_2V/Br^-$ flow battery manifested outstanding current performance, up to 78% energy efficiencies at 40 mA/cm^2 current density, and 227 mW/cm^2 power density, the highest power density known for pH neutral organic flow batteries.

Keywords: Redox Flow Batteries, Energy Storage, Viologen, Bromide, Redox Active Molecules

1. Introduction

To efficiently utilize the renewable energy source and achieve sustainable society, advanced large-scale energy storage technologies are highly demanded.[1-3] Among various energy storage devices, aqueous redox flow batteries (ARFBs) have been recognized as a suitable technology for large-scale energy storage.[2, 3] The ARFBs are characteristic of independent power and energy control, excellent rate performance and power generation, and inexpensive and nonflammable electrolytes, and thus well suited for the storage of intermittent and disperse renewable energy (e.g. wind and solar).[2, 3] However, traditional vanadium redox flow batteries (VRFBs) encounter several critical barriers for broad energy storage applications, including scarce and pricy vanadium resources, side-reactions (i.e. hydrogen and oxygen formation),

vanadium species crossover, and hazardous and corrosive strong acidic electrolytes.[2, 3] To realize affordable and sustainable electrochemical energy storage, low-cost organic and inorganic redox active materials has obtained increasing attention for RFB studies in recent years.[4-25]

Bromide are redox active inorganic materials which widely exist in nature (e.g. 65 mg/L in seawater, which is around 0.2% of all dissolved salts). Lots of bromide salts are highly soluble in water with a high redox potential $E_{1/2}(Br_3^-/Br^-)$ at 1.08 V (vs. NHE). Zn/Br^- RFBs have been received massive studies and continuous commercialization.[26] However, the current and power performance of the Zn/Br^- RFBs is limited by the formation of Zn dendrites on the anode electrode.[26] In addition, power and energy are not fully decoupled in the hybrid Zn/Br^- systems because of the deposition/stripping of solid state zinc electrode.[2, 3] Meanwhile, to avoid the hydrolysis of Zn^{2+} cation, the electrolytes need to be kept under acidic pH, however, zinc anode corrosion due to H_2 evolution reaction is significant and leads to charge imbalance.[26] Other anode materials such as polysulfide (S_x^{2-}) and anthraquinone (AQ) derivatives were used to pair with the Br_3^-/Br^- redox couple for RFB application.[27-29] However, the crossover of sulfide limited the battery performance of S_x^{2-}/Br^- ARFBs,[3, 27] some AQ derivatives were degraded in the presence of Br_2 through bromination reactions.[28] Moreover, the AQ/Br^- ARFBs were demonstrated under corrosive strong acidic conditions (usually 3.0 M HBr).[8, 28] Thus, utilization of the low-cost, high redox potential bromide catholyte is highly desired in high performance benign pH neutral ARFBs, which remains unknown so far.

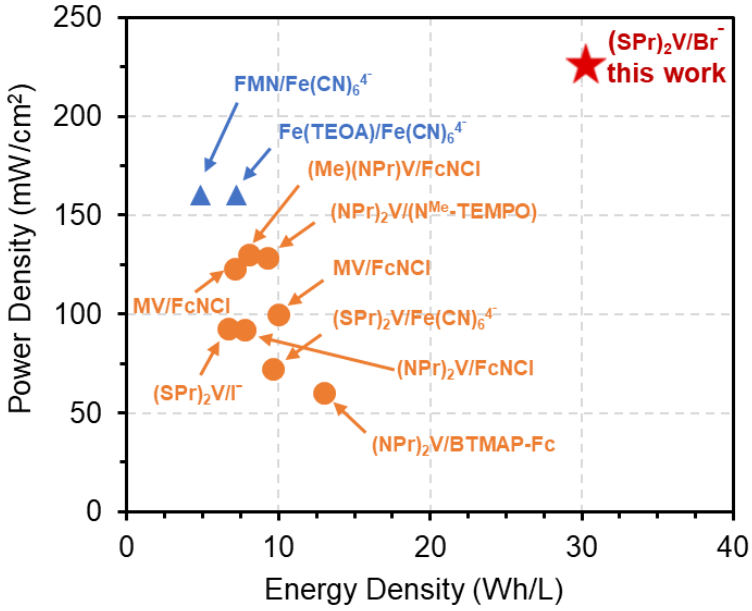

Figure 1. Comparison of the demonstrated energy density and power density of AORFB in this work and previously reported representative pH neutral (orange) and alkaline (blue) AORFBs. Neutral AORFBs: MV/FcNCl,[21,35] $(NPr)_2V/FcNCl$,[30] $(NPr)_2V/(N^{Me}$-TEMPO),[36] $(Me)(NPr)V/FcNCl$,[30] $(SPr)_2V/I^-$,[33] $(SPr)_2V/Fe(CN)_6^{4-}$,[34] and $(NPr)_2V/BTMAP$-Fc;[32] alkaline AORFBs: $FMN/Fe(CN)_6^{4-}$ [37] and $Fe(TEOA)/Fe(CN)_6^{4-}$.[38]

We and other groups have demonstrated that viologen molecules are privileged as highly stable tunable anolytes in aqueous organic redox flow batteries (AORFBs) at pH neutral conditions.[9, 10, 21, 30-32] However, the low redox potential and low solubility of catholytes limited energy (less than 13.0 Wh/L) and power (less than 130 mW/cm^2) densities of the related pH neutral AORFBs (Figure 1). High voltage and energy density was obtained by using N^{Me}-TEMPO catholyte, however, the cost of redox material is fairly high.[30, 31] Moreover, due to the relative low ion conductivity of pH neutral electrolytes, the power densities of the neutral AORFBs are still not competitive with those of strong alkaline and acidic RFBs.[8, 22] Herein, we exploit the high redox potential (1.08 V vs NHE) and high capacity (8.0 M or 214.4 Ah/L) ammonium bromide catholyte, NH_4Br, in pH neutral AORFB for the first time by pairing with 1,1'-bis(3-sulfonatopropyl)-4,4'-bipyridinium ($(SPr)_2V$) as an anolyte.[33, 34] With the high solubility of both $(SPr)_2V$ [33, 34] and NH_4Br and their large redox gap (1.51 V), a high operational energy density of 30.4 Wh/L was achieved for the $(SPr)_2V/Br^-$ AORFB, among most energy dense AORFBs. Using multiwall carbon nanotubes (MWCNTs) as electrode additive to improve

the electrochemical kinetics of Br_3^-/Br^- redox couple, a 1.5 M $(SPr)_2V/Br^-$ AORFB was able to cycle at 40 - 100 mA/cm^2 with up to an energy efficiency of 78% and coulombic efficiency (CE) of > 98%. Notably, the 1.5 M $(SPr)_2V/Br^-$ AORFB delivered a power density of 227 mW/cm^2 even at pH neutral conditions, which is the highest value known for the pH neutral AORFBs, and it is even higher than some strong alkaline AORFBs (Figure 1).[21, 30, 32-38] The low cost, high energy and power densities of the $(SPr)_2V/Br^-$ AORFB marks it promising for scalable renewable energy storage.

2. Experimental Procedures

Chemicals and Manipulations: Chemicals were purchased from Sigma-Aldrich or TCI Chemicals, stored in an argon glovebox and used directly. $(SPr)_2V$ was synthesized and characterized as reported previously by us.[33, 34] DI water was purged overnight using N_2 before use. All batteries were tested under N_2 atmosphere; the pH values of electrolytes were adjusted to 7.0 using diluted HCl or $NH_3{\bullet}H_2O$. Conductivities and pH values of the electrolytes were measured using a Mettler Toledo conductivity meter or a Mettler Toledo pH meter at room temperature. ^{1}H-NMR spectrum were collected using a Bruker 500 MHz NMR spectrometer. All electrochemical experiments were conducted with a Gamry 1000E or 5000E potentiostat. Battery tests were performed using a Land battery testing system.

Cyclic Voltammetry Studies: A Gamry 1000E potentiostat was used to perform the CV tests with using a three-electrode system in a 0.5 M NH_4Cl electrolyte solution under N_2 atmosphere. A PEEK-encased 3 mm diameter glassy carbon or Pt disk was used as working electrode. A glassy carbon rod was used as the counter electrode. An Ag/AgCl reference electrode was constructed by submerging a silver wire in 3.0 M KCl solution. Before each test, the working electrode was polished with 0.05 micron alumina powder and rinsed with DI water. Potential values were corrected to NHE using (ferrocenylmethyl)trimethylammonium chloride (FcNCl) internal standard with a known redox potential at 0.61 V vs. NHE. The scan rate for all the CV tests in this study were 100 mV/s.

Half-cell Flow Battery Tests: The half-cell flow battery for the $(SPr)_2V/(SPr)_2V^{-\cdot}$ redox couple was constructed with two carbon electrolyte chambers, two graphite felt electrodes (SGL Carbon Group, Germany), a piece of cation-exchange membrane (Nafion ® 212 membrane) as separator sandwiched between graphite felts, and two copper plates as current collectors. Each carbon

chamber was connected with an electrolyte reservoir using a piece of Viton tubing. The electrolyte reservoir is homemade and is a 10 mL glass tube (2 cm inner diameter). The effective area of the cell was 10 cm^2. The circulation of the electrolytes was implemented by a Masterflex L/S peristaltic pump (Cole-Parmer, Vernon Hills, IL) at a flow rate of 60 mL/min. Each reservoir contains 12 mL of 1.0 M NH_4Cl electrolytes containing 0.5 M active materials. Before cell cycling, nitrogen flow was used to purge the reservoirs to remove O_2. The flow cell was charged/discharged galvanostatically at room temperature on a Land battery tester in the voltage window of -0.25 − 0.25 V at current densities of 40, 60, 80, and 100 mA/cm^2. Post cell analysis of the electrolytes after fully discharge using ^{1}H-NMR and CV at the end of 500 cycles of tests.

Full-cell Flow Battery Tests: The setup of the $(SPr)_2V/Br$ AORFBs is the same as the $(SPr)_2V/(SPr)_2V^{-\cdot}$ half-cell battery. For the 0.1 M RFB: 12.0 ml of 0.1 M $(SPr)_2V$ in 1.0 M NH_4Br solution was used as an anolyte, 0.1 M Br_2 in 1.2 M NH_4Br solution was used as a catholyte, a piece of Nafion® 212 membrane was used as a separator. For the 1.0 M RFB: 12.0 ml of 1.0 M $(SPr)_2V$ in 1.5 M NH_4Br solution was used as an anolyte, 0.2 M Br_2 in 3.5 M NH_4Br solution was used as catholyte, a piece of Nafion® 115 membrane was used as a separator. For the 1.5 M RFB: 12.0 ml of 1.5 M $(SPr)_2V$ in 1.0 M NH_4Br solution was used as an anolyte, 0.2 M Br_2 in 4.0 M NH_4Br solution was used as a catholyte, a piece of Nafion® 115 membrane was used as separator. The cell was galvanostatically charged to 1.7 or 1.8 V and discharged to 0.1 V at current densities ranging from 40 to 100 mA/cm^2.

Preparation of MWCNT-Modified Glassy Carbon Electrode (GCE): The multiwall carbon nanotube (MWCNT)-modified GCE was prepared as the literature reported.[39] In brief, 2.5 mg of MWCNTs were dispersed in 750 μL of deionized water and isopropanol (1:5 ratio) mixture by ultra-sonication. Thirty microliters of MWCNT slurry was dropped onto the polished GCE and dried at ambient condition for 30 min to evaporate the solvent completely.

Preparation of MWCNT-Loaded Graphite Felt Electrodes (MWCNT@GF): The MWCNT@GF electrode was prepared using a similar procure as previously reported.[39] Typically, a graphite felt electrodes (SGL Carbon Group, Germany) (10 cm^2) was subjected to ultra-sonication in deionized water and dried at 60 °C for 5 h. A 1:1 weight and volume ratio of MWCNTs and DMF were mixed together by ultra-sonication for about 10 min. The pretreated GF was immersed in MWCNT−DMF solution and subjected to ultra-sonication for 2 hours. The

MWCNT-loaded GF was dried at 100 °C for 24 h and weight changes indicated a loading of 0.8 mg/cm^2.

3. Results and Discussion

Among common bromide salts (NH_4Br, NaBr, and KBr), ammonium bromide displayed high solubility/charge capacity and its aqueous solution also has high molar conductivity. In addition, ammonium cation (NH_4^+) has a charge mobility comparable with K^+ but faster than Na^+ through a cation exchange membrane.[34] These advantageous physical properties highlights NH_4Br is an optimal choice of redox active bromide catholyte for pH neutral AORFBs. The cyclic voltammogram of NH_4Br in 0.5 M NH_4Cl water solutions displays a reversible oxidation wave at 1.08 V vs NHE (Scheme 1 and Figure 2A), the combination of NH_4Br with $(SPr)_2V$ (-0.43 V vs NHE) gives a battery voltage of 1.51 V, which is bracketed within the electrochemical window of water (HER at -1.43 and OER at 1.30 V, Figure S1). In addition, the electrochemical and chemical stability of the $(SPr)_2V$ anolyte in NH_4Cl was studied in a symmetric half-cell RFB using $(SPr)_2V$ and $(SPr)_2V^{-\cdot}$ in anode and cathode side, respectively. As shown in Figure S2, a 0.5 M $(SPr)_2V/(SPr)_2V^{-\cdot}$ half-cell RFB was tested using cut-off voltages of -0.25 and 0.25 V in a current density range of 40 – 100 mA/cm^2. Under each current density, the half-cell battery delivered stable charge/discharge profiles and nearly 100% CE. To confirm the long-term durability of the $(SPr)_2V/(SPr)2V^{-\cdot}$ couple, 500 cycle data was collected at 60 mA/cm^2 using the half-cell battery. No capacity fading was observed during the battery cycling which indicated excellent chemical stability of $(SPr)_2V/(SPr)_2V^{-\cdot}$ redox couple. It was further confirmed by the CV and ^{1}H-NMR post cycling analysis (Figure S3 and S4).

The $(SPr)_2V/Br^-$ full-cell AORFB was first demonstrated using 0.1 M $(SPr)_2V$ in 1.0 M NH_4Br aqueous solution as anolyte and 0.1 M Br_2 in 1.2 M NH_4Br aqueous solution as catholyte,

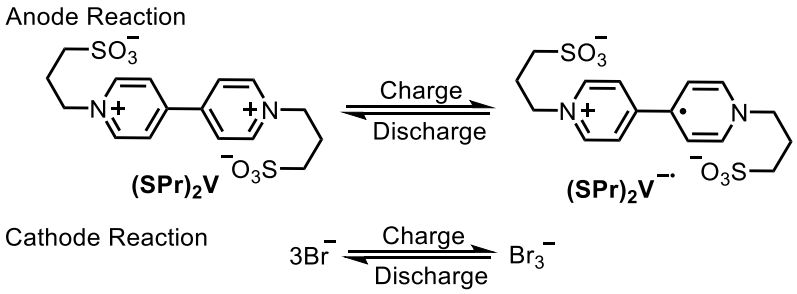

Scheme 1. The scheme of anode and cathode half-cell reactions for the $(SPr)_2V/Br^-$ AORFB.

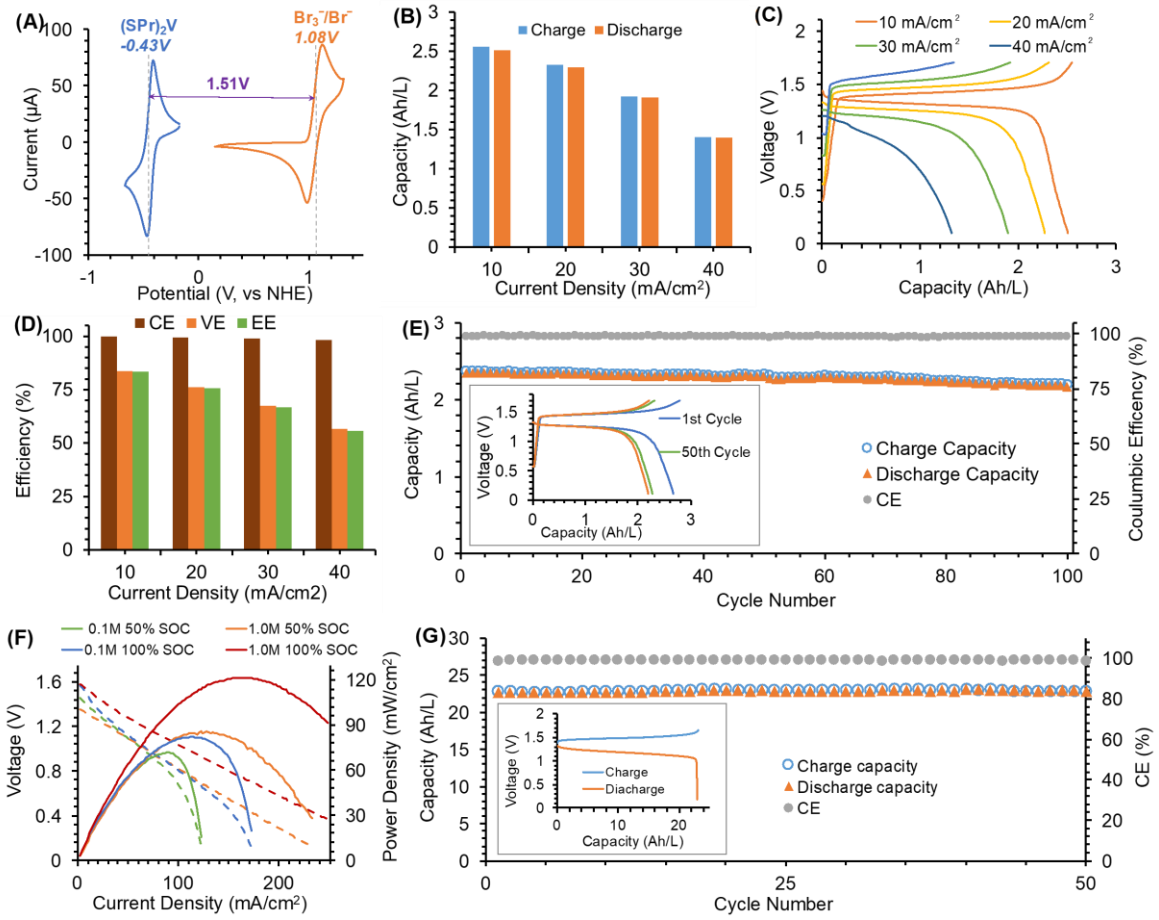

Figure 2. (A) Cyclic voltammogram curves of 50 mM NH_4Br (1.08 V) or 4.0 mM $(SPr)_2V$ (-0.43 V) in 0.5 M NH_4Cl water solution (glassy carbon working electrode for $(SPr)_2V$ and Pt working electrode for NH_4Br). (B) Averaged charge and discharge capacities of the 0.1 M $(SPr)_2V/Br^-$ AORFB at different current densities (5 data points were collected under each current density). (C) Capacity-voltage plots of the 0.1 M $(SPr)_2V/Br^-$ AORFB at four current densities as labelled. (D) Battery efficiencies (CE, EE, and VE) of the AORFB at each operational current density. (E) Charge/discharge capacity and CE of the 0.1 M AORFB showing for 100 cycles (20 mA/cm^2). Testing conditions: 0.1 M $(SPr)_2V$ in 1.0 M NH_4Br and 1.2 M NH_4Br with 0.1 M Br_2; Nafion 212; pH 7.0. (F) Power density (solid) and polarization (dash) plots of 0.1 M and 1.0 M $(SPr)_2V/Br^-$ AORFBs at 100% and 50% SOC. (G) Charge/discharge capacity and CE of the 1.0 M AORFB for 50 cycles (40 mA/cm^2). Inset: charge and discharge curves of the AORFB. Testing conditions: 1.0 M $(SPr)_2V$ in 1.5 M NH_4Br and 3.5 M NH_4Br with 0.2 M Br_2; Nafion 115; pH 7.0.

and a Nafion 212 cation-exchange membrane as the separator for NH_4^+ cation exchange. Herein, we chose NH_4^+ as charge carrier for battery charge/discharge, due to its higher ion conductivity than Na^+ and K^+ in Nafion 212 cation-exchange membrane (Figure S5). Figure 2 displays the performance of the 0.1 M $(SPr)_2V/Br^-$ AORFB. The flow battery was first evaluated at four current densities of 10, 20, 30, and 40 mA/cm^2 within the charge/discharge voltage window between 0.1 and 1.7 V. At each current density, the battery delivered up to 97% capacity utilization at 10 mA/cm^2 current density and > 98% CE (Figure 2B and 2D). Meanwhile, satisfactory VE and EE were obtained, i.e., 83% VE and EE at 10 mA/cm^2. They retained 57% when the current was augmented to 40 mA/cm^2 (Figure 2D). The cycling stability of the 0.1 M $(SPr)_2V/Br^-$ AORFB was measured at 20 mA/cm^2. 7.1% capacity fading was observed after 100 charge/discharge cycles (30 hours), giving capacity stability of 99.93% for each cycle or 99.76% for each hour (Figure 2E). The average CE of the AORFB is 98.88%, slightly lower than 100% due to the crossover of Br_2 from the cathode side to the anode side.

To mitigate the crossover of Br_2 in the $(SPr)_2V/Br^-$ AORFBs, a thicker Nafion 115 cation-exchange membrane was used as a separator and the $(SPr)_2V$ concentration was increased to 1.0 M. As shown in Figure 2G, 1.0 M $(SPr)_2V$ in 1.5 M NH_4Br was used as anolyte, 0.2 M Br_2 in 3.5 M NH_4Br was used as catholyte, the AORFB was charge/discharged between 1.7 V and 0.1 V under 40 mA/cm^2 current density for 50 cycles without observing capacity decay (75 hours, 100% retention for each cycle or 100% retention for each hour). The AORFB delivered impressive electrochemical performance, including 80% EE, 81% VE, and 99.12% CE, in average. ^{1}H-NMR measurement was conducted to the anolyte after fully discharge of the battery. As shown in Figure S6, the ^{1}H-NMR spectrum of the $(SPr)_2V$ kept unchanged after 50 charge/discharge cycles, which indicates no chemical degradation of $(SPr)_2V$ under the battery condition. Polarization studies of the 0.1 and 1.0 M $(SPr)_2V/Br^-$ AORFBs were conducted at 100% and 50% SOC. As shown in Figure 2F, a significant improvement of power density was observed when the electrolyte concentration increase from 0.1 M to 1.0 M (121.4 mW/cm^2 at 100% SOC and 85.6 mW/cm^2 at 50% SOC for the 1.0 M AORFB, and 82.0 mW/cm^2 at 100% SOC and 71.6 mW/cm^2 at 50% SOC for the 0.1 M AORFB). Meanwhile, the open circuit voltage (OCV) of both batteries were 1.57 V at 100% SOC.

To further boost energy density of the $(SPr)_2V/Br^-$ AORFB, the concentration of the $(SPr)_2V$ anolyte was further increased to 1.5 M (30.35 Wh/L operational energy density).

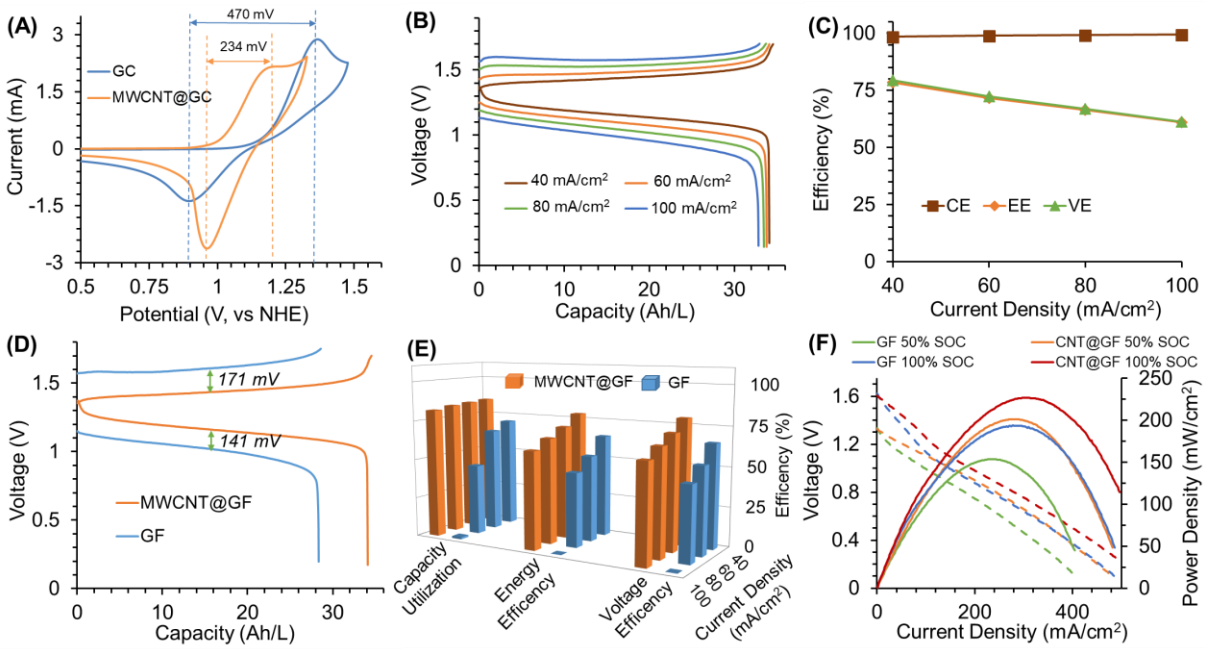

Figure 3. (A) Cyclic voltammograms of 50 mM NH_4Br in 0.5 M NH_4Cl on glassy carbon (GC) working electrode (blue) and MWCNT modified GC working electrode (orange). (B) Capacity-voltage plots of the 1.5 M $(SPr)_2V/Br^-$ AORFB at four current densities. (C) Battery efficiencies of the AORFB at each current density. (D) Charge/discharge curves of the 1.5 M $(SPr)_2V/Br^-$ AORFBs using MWCNT@GF (orange) and bare GF (blue) as cathode at 40 mA/cm^2. (E) Capacity utilization and battery efficiencies comparison of the 1.5 M $(SPr)_2V/Br^-$ AORFBs using MWCNT@GF (orange) and bare GF (blue) as cathode under various current densities. (F) Power density (solid) and polarization (dash) plots at 100% and 50% SOC of the 1.5 M $(SPr)_2V/Br^-$ AORFBs using MWCNT@GF and bare GF as cathode. Testing conditions: 1.5 M $(SPr)_2V$ in 1.0 M NH_4Br and 4.0 M NH_4Br with 0.2 M Br_2; Nafion 115; pH 7.0.

However, due to the poor electrochemical kinetics of Br_3^-/Br^- redox couple on the carbon electrode and low conductivity of the highly concentrated $(SPr)_2V$ solution (31.0 mS/cm conductivity of 1.5 M $(SPr)_2V$ in 1.0 M NH_4Br), the corresponding AORFB delivered high charge/discharge over-potential and poor efficiencies (Figure S7). Carbon nanotubes (CNTs) have been reported to facilitate the Br_3^-/Br^- redox couple.[39, 40] Herein, multiwall carbon nanotubes (MWCNTs) were loaded as an efficient electrode additive into the cathode side graphite felt electrode to promote the energy efficiency and power density of the battery. The

activity of MWCNTs to enhance the Br_3^-/Br^- redox couple was first investigated by CV measurement. As shown in Figure 3A, the electrochemical reversibility and kinetics of Br_3^-/Br^- redox couple was significantly improved by the MWCNT modification of the glassy carbon electrode, specifically, the peak-peak separation was reduced from 470 mV to 234 mV, the oxidative and reductive peak current ratio (I_{pO}/I_{pR}) was reduced from 2.1 to 0.83 (it is more near to 1.0). The MWCNT loaded graphite felt (MWCNT@GF) was used as cathode electrode for the 1.5 M $(SPr)_2V/Br^-$ AORFB. As shown in Figure 3B, the AORFB displayed excellent current rate performance, only 3.7% capacity decrease was observed with the current density increase from 40 mA/cm^2 to 100 mA/cm^2. Meanwhile, the battery delivered high efficiencies, specifically, 79% VE and EE at 40 mA/cm^2, and they still retained 61% when the operational current density was even increased to 100 mA/cm^2 (Figure 3C). The cycling stability of the 1.5 M $(SPr)_2V/Br^-$ battery was tested using 80 mA/cm^2 for 30 cycles. The highly energy dense AORFB is fairly stable, 99.90% retention for each cycle or 99.89% retention for each hour with 99.5% average coulombic efficiency was observed (Figure S8).

The battery performance of the 1.5 M $(SPr)_2V/Br^-$ AORFB was significantly improved by using the MWCNT additive in the cathode electrode. As displayed in Figure 3D, charge and discharge over-potentials of the $(SPr)_2V/Br^-$ flow battery using the MWCNT@GF electrode were reduced by around 171 mV and 141 mV, respectively. Under the same current range, the $(SPr)_2V/Br^-$ AORFB with the MWCNT@GF electrode displayed much better efficiencies than the one using the unmodified GF electrode (Figure 3E). For example, the $(SPr)_2V/Br^-$ AORFB with MWCNT@GF delivered 84.8% capacity utilization, 79% VE, and 78% EE at 40 mA/cm^2 (Figure 3E, orange plot), much higher than those (70% capacity utilization, 65% EE, and 65% VE) of the AORFB using unmodified GF electrode (Figure 3E, blue plot, also Figure S7). In addition, the battery with the MWCNT@GF cathode electrode delivered much higher power densities than the one using the unmodified GF cathode electrode, for example, 227 mW/cm^2 and 201 mW/cm^2 power densities at 100% and 50% SOC, respectively, for the one using the MWCNT@GF cathode electrode; 198 mW/cm^2 and 162 mW/cm^2 power densities at 100% and 50% SOC, respectively, for the one using the unmodified GF cathode electrode. EIS measurements were conducted for an in-depth understanding of activation mechanism of Br_3^-/Br^- by MWCNTs. As shown in Figure S9, the charge transfer resistance of the battery was decreased from 33 Ω•cm^2 to 14 Ω•cm^2 by using the MWCNT additive. It can be explained that

MWCNTs with high surface area can supply more active sites for the Br_3^-/Br^- redox reaction that induces improved electrochemical kinetics to minimize electrochemical polarization.[39]

As above mentioned, the bromide catholyte materials have several advantages, such as abundance, low-cost, and high redox potential. However, the Br_2-based RFB is still very challenging. On the one hand, the Br_2 is highly corrosive and volatile. The volatilization of hazardous Br_2 will induce unbalance of matter and charge that affect the cycling performance of the RFB. And there are also environmental and health concerns. On the other hand, there is a chemical equilibrium between Br_3^- anion and neutral Br_2 in the aqueous solution. The small neutral Br_2 molecules could easily crossover through the separator to react with the anolyte that will induce CE loss and irreversible capacity fading.[41] Some solutions have been reported to address these issues. For example, to solve the Br_2 volatilization issue, complexing reagents such as quaternary ammonium bromides can be used to trap the Br_3^- anion, then the liquid Br_2 volume and its vapor pressure can be minimized.[42-44] The addition of complexing reagents can also slow down the crossover of the Br_2 species. Additionally, advanced cation-exchange membranes to suppress the bromine crossover are highly demanded for the Br-based ARFBs.[45] Besides these two options, bipolar electrolytes and symmetric battery design can also be considered. It is clear that there is a wide designing space to further improve the electrochemical performance of the $(SPr)_2V/Br^-$ AORFB. For instance, an ongoing effort in our lab is to identify complexing agents to stabilize the Br_3^-/Br^- catholyte.

4. Conclusion

In summary, low-cost, high potential ammonium bromide catholyte was applied in the pH neutral AORFB for the first time. A 1.51 V pH neutral $(SPr)_2V/Br^-$ AORFB was demonstrated at a high concentration of 1.5 M with an energy density of 30.35 Wh/L. Using the MWCNT electrode additive for the Br_3^-/Br^- redox couple, the 1.5 M $(SPr)_2V/Br^-$ AORFB delivered up to 78% EE and 227 mW/cm^2 power density at 100% SOC, which is the highest power density value ever reported for pH neutral AORFBs. The low cost, high energy and power densities of the violoen/Br^- flow battery reported in this work hold a viable potential for economical and sustainable storage of renewable energy.

Supplemental Information includes experimental procedures, post-cell NMR and CV analysis, cell impedance spectroscopy, battery data. Supplemental information can be obtained openly in the online version.

Acknowledgement

We thank the financial support for this research from National Science Foundation Career Award (Grant No. 1847674), faculty startup funds from Utah State University and the Utah Science Technology and Research initiative (USTAR) UTAG award. C.D. is grateful for the USU Presidential Doctoral Research Fellowship supported by USU. B.H. is grateful for the China CSC Abroad Studying Fellowship and the Utah Energy Triangle Student Award supported by the Office of Energy of the Utah State government to support his graduate program. M.H. is grateful for the China CSC Abroad Studying Fellowship to support her graduate program.

Author Contributions

T. L. L. designed the project. J. L. conducted experiments. W. W. helped on collecting and analyzing the battery data. T. L. L., J. L. analyzed experimental data and prepared the manuscript, and all authors contributed to revising the manuscript.

Declaration of Interests

A patent application was submitted based on the results reported herein.

References:

1. B. Dunn, H. Kamath and J.-M. Tarascon, *Science*, 2011, **334**, 928-935.
2. Z. Yang, J. Zhang, M. C. W. Kintner-Meyer, X. Lu, D. Choi, J. P. Lemmon and J. Liu, *Chem. Rev.*, 2011, **111**, 3577-3613.
3. G. L. Soloveichik, *Chem. Rev.*, 2015, **115**, 11533-11558.
4. J. Winsberg, T. Hagemann, T. Janoschka, M. D. Hager and U. S. Schubert, *Angew. Chem., Int. Ed.*, 2017, **56**, 686-711.
5. P. Leung, A. A. Shah, L. Sanz, C. Flox, J. R. Morante, Q. Xu, M. R. Mohamed, C. Ponce de León and F. C. Walsh, *J. Power Sources*, 2017, **360**, 243-283.
6. X. Wei, W. Pan, W. Duan, A. Hollas, Z. Yang, B. Li, Z. Nie, J. Liu, D. Reed, W. Wang and V. Sprenkle, *ACS Energy Lett.*, 2017, **2**, 2187-2204.
7. Y. Ding, C. Zhang, L. Zhang, Y. Zhou and G. Yu, *Chem. Soc. Rev.*, 2018, **47**, 69-103.
8. B. Huskinson, M. P. Marshak, C. Suh, S. Er, M. R. Gerhardt, C. J. Galvin, X. Chen, A. Aspuru-Guzik, R. G. Gordon and M. J. Aziz, *Nature*, 2014, **505**, 195.

9. T. Janoschka, N. Martin, U. Martin, C. Friebe, S. Morgenstern, H. Hiller, M. D. Hager and U. S. Schubert, *Nature*, 2015, **527**, 78.
10. T. Liu, X. Wei, Z. Nie, V. Sprenkle and W. Wang, *Adv. Energy Mater.*, 2016, **6**, 1501449.
11. J. D. Milshtein, A. P. Kaur, M. D. Casselman, J. A. Kowalski, S. Modekrutti, P. L. Zhang, N. Harsha Attanayake, C. F. Elliott, S. R. Parkin, C. Risko, F. R. Brushett and S. A. Odom, *Energy Environ. Sci.*, 2016, **9**, 3531-3543.
12. L. Zhang, C. Zhang, Y. Ding, K. Ramirez-Meyers and G. Yu, *Joule*, 2017, **1**, 623-633.
13. C. S. Sevov, D. P. Hickey, M. E. Cook, S. G. Robinson, S. Barnett, S. D. Minteer, M. S. Sigman and M. S. Sanford, *J. Am. Chem. Soc.*, 2017, **139**, 2924-2927.
14. A. Hollas, X. Wei, V. Murugesan, Z. Nie, B. Li, D. Reed, J. Liu, V. Sprenkle and W. Wang, *Nature Energy*, 2018, **3**, 508-514.
15. M. Zhou, Q. Huang, T. N. Pham Truong, J. Ghilane, Y. G. Zhu, C. Jia, R. Yan, L. Fan, H. Randriamahazaka and Q. Wang, *Chem*, 2017, **3**, 1036-1049.
16. C. Yang, G. Nikiforidis, J. Y. Park, J. Choi, Y. Luo, L. Zhang, S.-C. Wang, Y.-T. Chan, J. Lim, Z. Hou, M.-H. Baik, Y. Lee and H. R. Byon, *Adv. Energy Mater.*, 2018, **8**, 1702897.
17. M. Burgess, K. Hernández-Burgos, J. K. Schuh, J. Davila, E. C. Montoto, R. H. Ewoldt and J. Rodríguez-López, *J. Am. Chem. Soc.*, 2018, **140**, 2093-2104.
18. W. Li, H.-C. Fu, Y. Zhao, J.-H. He and S. Jin, *Chem*, 2018, **4**, 2644-2657.
19. J. Huang, L. Cheng, R. S. Assary, P. Wang, Z. Xue, A. K. Burrell, L. A. Curtiss and L. Zhang, *Adv. Energy Mater.*, 2015, **5**, 1401782.
20. J. Huang, Z. Yang, V. Murugesan, E. Walter, A. Hollas, B. Pan, R. S. Assary, I. A. Shkrob, X. Wei and Z. Zhang, *ACS Energy Lett.*, 2018, **3**, 2533-2538.
21. B. Hu, C. DeBruler, Z. Rhodes and T. L. Liu, *J. Am. Chem. Soc.*, 2017, **139**, 1207-1214.
22. K. Lin, Q. Chen, M. R. Gerhardt, L. Tong, S. B. Kim, L. Eisenach, A. W. Valle, D. Hardee, R. G. Gordon, M. J. Aziz and M. P. Marshak, *Science*, 2015, **349**, 1529-1532.
23. Y. Ding, C. Zhang, L. Zhang, H. Wei, Y. Li and G. Yu, *ACS Energy Lett.*, 2018, **3**, 2641-2648.
24. C. Zhang, Z. Niu, Y. Ding, L. Zhang, Y. Zhou, X. Guo, X. Zhang, Y. Zhao and G. Yu, *Chem*, 2018, **4**, 2814-2825.
25. C. Zhang, L. Zhang, Y. Ding, S. Peng, X. Guo, Y. Zhao, G. He and G. Yu, *Energy Storage Mater.*, 2018, **15**, 324-350.
26. A. Khor, P. Leung, M. R. Mohamed, C. Flox, Q. Xu, L. An, R. G. A. Wills, J. R. Morante and A. A. Shah, *Mater. Today Energy*, 2018, **8**, 80-108.
27. C. Ponce de León, A. Frías-Ferrer, J. González-García, D. A. Szánto and F. C. Walsh, *J. Power Sources*, 2006, **160**, 716-732.
28. M. R. Gerhardt, L. Tong, R. Gómez-Bombarelli, Q. Chen, M. P. Marshak, C. J. Galvin, A. Aspuru-Guzik, R. G. Gordon and M. J. Aziz, *Adv. Energy Mater.*, 2017, **7**, 1601488.
29. R. J. Remick and P. G. P. Ang, *U.S. Patent 4485154*, 1984.
30. C. DeBruler, B. Hu, J. Moss, X. Liu, J. Luo, Y. Sun and T. L. Liu, *Chem*, 2017, **3**, 961-978.
31. T. Janoschka, N. Martin, M. D. Hager and U. S. Schubert, *Angew. Chem., Int. Ed.*, 2016, **55**, 14427-14430.
32. E. S. Beh, D. De Porcellinis, R. L. Gracia, K. T. Xia, R. G. Gordon and M. J. Aziz, *ACS Energy Lett.*, 2017, **2**, 639-644.
33. C. DeBruler, B. Hu, J. Moss, J. Luo and T. L. Liu, *ACS Energy Lett.*, 2018, **3**, 663-668.

34. J. Luo, B. Hu, C. Debruler, Y. Bi, Y. Zhao, B. Yuan, M. Hu, W. Wu and T. L. Liu, *Joule*, 2018.
35. B. Hu, C. Seefeldt, C. DeBruler and T. L. Liu, *J. Mater. Chem. A*, 2017, **5**, 22137-22145.
36. B. Hu, Y. Tang, J. Luo, G. Grove, Y. Guo and T. L. Liu, *Chem. Commun.*, 2018, **54**, 6871-6874.
37. A. Orita, M. G. Verde, M. Sakai and Y. S. Meng, *Nature Commun.*, 2016, **7**, 13230.
38. K. Gong, F. Xu, J. B. Grunewald, X. Ma, Y. Zhao, S. Gu and Y. Yan, *ACS Energy Lett.*, 2016, **1**, 89-93.
39. Y. Munaiah, S. Suresh, S. Dheenadayalan, V. K. Pillai and P. Ragupathy, *J. Phys. Chem. C*, 2014, **118**, 14795-14804.
40. Y. Munaiah, S. Dheenadayalan, P. Ragupathy and V. K. Pillai, *ECS J. Solid State Sci. Technol.*, 2013, **2**, M3182-M3186.
41. G. Li, Y. Jia, S. Zhang, X. Li, J. Li and L. Li, *J. Appl. Electrochem.*, 2017, **47**, 261-272.
42. Q. Lai, H. Zhang, X. Li, L. Zhang and Y. Cheng, *J. Power Sources*, 2013, **235**, 1-4.
43. D. J. Eustace, *J. Electrochem. Soc.*, 1980, **127**, 528-532.
44. J.-D. Jeon, H. S. Yang, J. Shim, H. S. Kim and J. H. Yang, *Electrochim. Acta*, 2014, **127**, 397-402.
45. B. Huskinson, M. P. Marshak, M. R. Gerhardt and M. J. Aziz, *ECS Trans.*, 2014, **61**, 27-30.

Graphical Abstract

A 1.51 V pH neutral $(SPr)_2V/Br^-$ AORFB with high energy and power densities was demonstrated for scalable energy storage.